Research Article

Cancer Immunology Research

Mitochondrial Morphological and Functional Reprogramming Following CD137 (4-1BB) Costimulation

Alvaro Teijeira[1,2], Sara Labiano[1], Saray Garasa[1], Iñaki Etxeberria[1], Eva Santamaría[1,3], Ana Rouzaut[1,2], Michel Enamorado[4], Arantza Azpilikueta[1,2], Susana Inoges[1], Elixabet Bolaños[1,2], Maria Angela Aznar[1], Alfonso R. Sánchez-Paulete[1,2], David Sancho[4], and Ignacio Melero[1,2]

Abstract

T and NK lymphocytes express CD137 (4-1BB), a costimulatory receptor of the TNFR family whose function is exploitable for cancer immunotherapy. Mitochondria regulate the function and survival of T lymphocytes. Herein, we show that CD137 costimulation provided by agonist mAb and CD137L (4-1BBL) induced mitochondria enlargement that resulted in enhanced mitochondrial mass and transmembrane potential in human and mouse $CD8^+$ T cells. Such mitochondrial changes increased T-cell respiratory capacities and were critically dependent on mitochondrial fusion protein OPA-1 expression. Mass and function of mitochondria in tumor-reactive $CD8^+$ T cells from cancer-bearing mice were invigorated by agonist mAb to CD137, whereas mitochondrial baseline mass and function were depressed in CD137-deficient tumor reactive T cells. Tumor rejection induced by the synergistic combination of adoptive T-cell therapy and agonistic anti-CD137 was critically dependent on OPA-1 expression in transferred $CD8^+$ T cells. Moreover, stimulation of CD137 with CD137 mAb in short-term cultures of human tumor-infiltrating lymphocytes led to mitochondria enlargement and increased transmembrane potential. Collectively, these data point to a critical link between mitochondrial morphology and function and enhanced antitumor effector activity upon CD137 costimulation of T cells. *Cancer Immunol Res; 6(7); 798–811. ©2018 AACR.*

Introduction

Mitochondria critically regulate metabolism and apoptosis in T cells, prompting the growing interest in how modulation of mitochondrial metabolism and dynamics can control T-cell function, survival, and memory differentiation (1, 2). This is the case of T cells within the tumor microenvironment, where the limiting concentration of some metabolites that are consumed by tumor cells influences T-cell metabolism and function (1, 3).

Costimulation is a concept that covers a set of functional consequences following ligation of T-cell surface receptors that act in conjunction with the T-cell antigen receptor (TCR; ref. 4). CD28 is the canonical T-cell costimulatory molecule expressed at baseline, with functions linked to anabolic metabolism and increased glycolysis, as well as mitochondrial respiration (5). CD137 (4-1BB) is a surface-TNFR family member whose expression is induced on primed T lymphocytes and provides important costimulatory signals (6). Experiments in $CD137^{-/-}$ mice show that 4-1BB plays a role in antiviral immunity (7). Its ligation with agonist moieties, such as mAbs, its natural ligand 4-1BBL, or RNA aptamers, enhances CTL-mediated antitumor immunity (8–10) as a result of multiple mechanisms (11, 12). Such functions are being exploited in cancer clinical trials with the agonist mAbs urelumab and utomilumab (13–15). Ligation of CD137 promotes both glycolysis and fatty acid synthesis (16). The cytoplasmic tail of CD137 has been introduced in clinically successful anti-CD19 chimeric antigen receptors (CAR; refs. 17, 18). In this setting, the inclusion of the CD137 cytoplasmic tail results in increased mitochondrial biogenesis and a more powerful respiratory capacity as compared to CARs containing the CD28 signaling domain (19).

Exhausted T lymphocytes, which express CD137 on their surface (20), are defective in mitochondria (21). Enhanced mitochondrial function has been linked to augmented $CD8^+$ T-cell effector and memory functions (22, 23). Intratumoral T lymphocytes are dysfunctional and show hypomorphic mitochondrial mass (24). Treatment with blocking mAbs to PD-1 increases T-cell mitochondrial content and functionality in mouse tumor models (25). Robust mitochondria in T cells give rise to a more efficacious antitumor performance, as shown in adoptive T-cell therapy experiments (23, 26).

In this study, we found that T-cell costimulation via CD137 enhances mitochondrial mass and respiratory capacity in an OPA-1-dependent fashion. In line with these findings, CD137

[1]Center for Applied Medical Research (CIMA), University of Navarra, Pamplona, Spain. [2]CIBERONC, Centro Virtual de la Investigación Biomédica en red de Oncología, Madrid, Spain. [3]CIBEREHD, Centro Virtual de la Investigación Biomédica en red de Enfermedades Hepáticas y Digestivas, Madrid, Spain. [4]Centro Nacional de Investigaciones Cardiovasculares Carlos III (CNIC), Madrid, Spain.

Note: Supplementary data for this article are available at Cancer Immunology Research Online (http://cancerimmunolres.aacrjournals.org/).

A. Teijeira and S. Labiano contributed equally to this article.

Corresponding Authors: Alvaro Teijeira, CIMA, University of Navarra, Avenida Pio XII, 55. 31008 Pamplona, Spain. Phone: 0034-948-194700-3030; Fax: 0034-938-194700; E-mail: ateijeiras@unav.es; and Ignacio Melero, imelero@unav.es

doi: 10.1158/2326-6066.CIR-17-0767

costimulation augments the mitochondrial mass and function of antitumor CD8$^+$ T cells in mice and humans.

Materials and Methods

Mice and cell lines

Female C57BL/6 wild-type mice (6–7 weeks old) were purchased from Harlan Laboratories. OT1, OT1-CD137KO-CD45.1, OT1-GFP, and C57BL/6 CD137KO (B6.Cg-Tnfrsf9^{tm1Byk}) mice were bred in our laboratory. All animal procedures were approved by the animal experimentation ethics committee of the regional government of Navarra (study 133/16).

MC38 cells were provided by Dr. Karl E. Hellström (University of Washington, Seattle, WA) in September 1998. B16-OVA cells were a kind gift from Dr. Lieping Chen (Yale University, New Haven, CT) in November 2001. Both cell lines were authenticated by Idexx Radil (Case 6592-2012) in February 2012. Cell lines were cultured in complete media containing RPMI 1640 medium (Gibco) supplemented with 10% FBS (Sigma-Aldrich), 100 IU/mL penicillin and 100 μg/mL streptomycin (Gibco) and 5×10^{-5} mol/L 2-mercaptoethanol (Gibco) for 7 days before injection into mice (2 expansion passages). B16-OVA cultures were supplemented with geneticin (400 μg/mL, Gibco).

In vitro CD8$^+$ T-lymphocyte costimulation assay

Mouse CD8 T lymphocytes were isolated from total splenocytes of C57BL/6 mice with CD8$^+$ T cell isolation kit (Miltenyi Biotec). Afterward, CD8$^+$ T cells were costimulated with plate-bound anti-CD3ε (0.5 μg/mL, clone 145-2C11, BioLegend) and anti-CD137 (10 μg/mL, clone 1D8) at 2.5×10^6 cells/mL for 72 hours in complete culture media.

Human CD8$^+$ T lymphocytes were obtained from peripheral blood mononuclear cells (PBMC) of healthy donors isolated from total blood by Ficoll gradients, following a negative magnetic selection with CD8$^+$ T cell isolation kit (Miltenyi Biotec). T lymphocytes were costimulated with plate-bound anti-CD3ε (0.5 μg/mL, clone OKT3) and anti-CD137 (10 μg/mL, clone 6B4 or urelumab) or the respective isotype control antibodies at 2.5×10^6 cells/mL for 72 hours in complete media. In some experiments, plate-bound anti-CD3 (0.5 μg/mL) and 4-1BBL or GAG protein-coated beads (ratio 1.2) were used (27). In some experiments, CD8$^+$ T cells were additionally costimulated with plate-bound anti-CD28 (10 μg/mL, clone 37.51) in the presence or absence of anti-CD137.

In cytokine supplementation/blockade experiments, human purified CD8 T cells were activated for 24 hours with 1 μg/mL plate-bound anti-CD3. Then, cells were added on top of plate bound anti-CD3 plus anti-CD137 or isotype control and supplemented with 100 IU/mL IL2, 10 ng/mL IFNγ (Miltenyi), or with 2.5 μg/mL anti-IL2 (Clone #5334, MAB202) or anti-IFNγ blocking mAb (clone #25718, MAB285; both from R&D Systems). The Akt inhibitor MK-2206 (Selleck Biochemicals) was added at a concentration of 100 nmol/L 24 hours after starting culture with plate bound anti-CD3/anti-CD137 and cells were collected for analysis 48 hours later.

Flow cytometry and cell sorting

For flow cytometry studies activated mouse CD8$^+$ T cells and single-cell suspensions from tumors and lymph nodes were previously treated with FcR-Block (anti-CD16/32 clone 2.4G2; BD Biosciences Pharmingen). T-cell suspensions were then surface stained with the following antibodies purchased from BioLegend: CD8-BV510, APC (53-6.7), CD137-PE (17B5), CD25-FITC (7D4), CD45.1-PerCPC5.5 (A20), CD45.2-APC (104), CD44-FITC (IM7), CD62L-APC (MEL-14), and mouse/human EOMES-PE (WD1928). For proliferation/apoptosis study, CD8$^+$ T cells were stained with CellTrace violet proliferation dye (Thermo Scientific) right after electroporation and costimulated for 72 hours. Cells were collected, suspended with 25 IU/mL IL7 and kept in culture for 7 additional days. Apoptosis was measured by staining of annexin V-APC (BD Biosciences Pharmingen) at the indicated time points. Cultured human CD8$^+$ T cells were pretreated with Beriglobin and stained with the following antibodies purchased from BD Bioscience and Biolegend: CD8-BV510 (5K1), CD137-PE (4B4-1), CD25-BV421 (BC96), CD45RA-PercP (HI100), PD-1-PercP (1A12), CD45.2 PB (104), Ki67-AlexaFluor488, IFNγ–APC (XMG1.2), TNFα-421 (MP6-XT22), and CD62L-PE (DERG-56). pS6 Riboprotein (S235/236)-Alexa Fluor 647 (D57.2.2E) was obtained from Cell Signaling Technologies.

For mitochondria staining, cells were incubated with a mitochondrial membrane potential indicator (TMRM; 125 ng/mL, Sigma) and MitoTracker deep red (10 nmol/L) or MitoTracker green (5 μmol/L; both from Thermo Scientific) in complete culture media for 20 minutes at 37°C. For intracellular staining of OPA-1, cells were fixed with PFA2% diluted in media at 37°C for 8 minutes. Subsequently, cells were washed and stained with OPA-1 in PBS 1% BSA 0.1% saponin for 1 hour. After two additional washes, cells were incubated with 1:200 anti-mouse IgG_1 Alexa 647 antibody (Thermo Scientific) for an additional hour. For pS6 staining, a BD Phosflow kit was used according to the manufacturer's instructions. For IFNγ, TNFα, and Ki67, the Cytofix/Cytoperm Kit (BD Biosciences) was used according to the manufacturer's instructions,

The Zombi NIR Fixable viability kit (BioLegend) was used as a live/dead marker. Cells were collected with FACSCanto II and FlowJo (TreeStar) software was used for data analysis.

For cell sorting–based experiments, CD8 T cells were magnetically purified from PBMCs from healthy donors and then stained with CD8, CD45RA, CD62L, or MitoTracker deep red (0.1 nmol/L). For MitoTracker-sorted experiments, cells were labeled with Cell Trace violet (Thermo Scientific) or CFSE (SIGMA) according to the manufacturer's instructions. Then cells were washed and put together to costimulate as explained above. In some experiments, after TMRM labeling, mouse T lymphocytes were sorted according to high or low fluorescence that correlated with the mitochondrial potential. All of these experiments were performed in a FACSAriaII cell sorter (BD Biosciences).

Transmission electron microscopy

After being fixed the samples in 2% paraformaldehyde, 2% glutaraldehyde in 0.1 mol/L sodium cocodylate in phosphate buffer, cells were washed in cocodylate buffer. A post-fixation step in 1% osmium tetroxide was applied for 2.5 hours. Cells were then stained with 2% aqueous uranyl acetate for 1 hour, following dehydration in ethanol (30°, 50°, 70°, 90°, 90°, Abs, Abs) and propilen oxide for 1 hour. Pre-embedded in 1:1 propilen oxide: epon and finally embedded in epon for 48 hours at 60°C (12 hours at 37°C, 12 hours at 45°C and 24 hours at 60°C). Thin sections of 50 nm were labeled with 2% uranyl acetate for 30 minutes at 37°C and lead citrate 15 minutes at room temperature. Images were taken with a Libra 120 energy filter transmission

electron microscope (EFTEM; Zeiss GmbH) using the software iTEM 5.1 (Olympus Soft Imaging Solutions GmbH).

Image analysis

Mitochondrial volume and number were measured using the Imaris (BitPlane) volume plugin. The person in charge of the analysis then inspected volumes, and manual corrections were made when individual mitochondria were not properly identified by the algorithm. Cross-sectional mitochondrial diameter was measured manually in ImageJ in confocal and TEM microphotographs.

RNA purification, reverse transcription, and qRT-PCR assays

Total RNA was extracted from purified CD8 T lymphocytes using a Maxwell 16LEV simplyRNA tissue kit (Promega). Reverse transcriptions were performed with M-MLV reverse transcriptase (Invitrogen) and quantitative RT-PCRs (qRT-PCR) were carried out with iQ SYBR green supermix in a CFX real-time PCR detection system (BioRad). PCRs included the following primers for human cells (*Drp-1*: fw: 5′-ATCTCATGGATGCGGGTACT-3′, rev: 5′-TTTCTATTGGCCAGAGATGGA-3′; *Fis 1*: fw: 5′-AGCGGGATTACGTCTTCTACC-3′, rev: 5′-CATGCCCACGAGTCCATCTTT-3′, *Mfn2* fwd: 5′-GGCCCAACTCTAAGTGCCC-3′, rev: 5′-AAGTGCTTTTCCGTCTGCATC-3′; *Mfn1*: fw: 5′-TGGCTAAGAAGGCGATTACTGC-3′, rev: 5′-TCTCCGAGATAGCACCTCACC-3′, *Nrf1*: fw: 5′-GCTGATGAAGACTCGCCTTCT-3′, rev: 5′-TACATGAGGCCGTTTCCGTTT-3′, *Nrf2*: fw: 5′-TTGGCAAGTCAAGAACAACAGA-3′, rev: 5′-GCGCTCTTTGTACTTTGGCT-3′; *Opa-1*: fw: 5′-TGTGATTGAAAACATCTACCTTCCA-3′, rev: 5′-TTTAAGCTTGATATCCACTGTGGTGT-3′; *Tfam*: fw: 5′-ATGGCGTTTCTCCGAAGCAT-3′, rev: 5′-TCCGCCCTATAAGCATCTTGA-3′; *Cpt1a*: fw: 5′- TTTGGACCGGTTGCTGATGA-3′. rev: 5′- TTTCCAGCCCAGCACATGAA-3′) and mouse cells (*Opa-1*: fw: 5′-TCCGCCCTATAAGCATCTTGA-3′, rev: 5′- CTTCCGCAGCTCTTTGTTCTC-3′; *Cpt1a* fw 5′- GACTCCGCTCGCTCATTCC-3′, rev: 5′- ACCAGTGATGATGCCATTCTTG-3′). Expression data were normalized by comparison with levels of H3 (mouse and human: fw: 5′-AAAGCCGCTCGCAAGAGTGCG-3′, rev: 5′-ACTTGCCTCCTGCAAAGCAC-3′). The expression of each transcript was represented according to this formula 2ΔCt (Ct H3 − Ct gene of interest), where Ct corresponds to cycle number.

In vivo tumor studies

Wild-type C57BL/6 and CD137KO C57BL/6 mice were inoculated subcutaneously in the flank with 5×10^5 MC38 colon carcinoma cells. At day 10 after tumor inoculation mice were sacrificed to obtain lymphocytes from tumors and draining (DLN) and nondraining lymph nodes (NDLN). For seahorse studies, total CD8 T cells were isolated from 10 pooled mice per condition by magnetic negative selection.

For adoptive T-cell transfer experiments, C57BL/6 mice were inoculated subcutaneously in the flank with 5×10^5 B16-OVA melanoma cells. At day 7 of tumor inoculation, mice were adoptively transferred with preactivated (16 hours activated with anti-CD3 at 1 μg/mL) OT1 CD137KO CD45.1 or OT1 GFP T cells and treated i.p. with 100 μg of anti-CD137 (clone 1D8) or the corresponding isotype control antibody. Three days later, mice were sacrificed to recover T lymphocytes from tumor, DLN, and NDLN. Isolated tumors were incubated with collagenase-D and DNase-I (Roche) for 15 minutes at 37°C, followed by mechanical disaggregation and filtration in a 70-μm cell strainer (BD Falcon, BD Biosciences). Tumor-infiltrating lymphocytes (TIL) were isolated from stromal cells in a 35% Percoll gradient. Lymph nodes were mechanically disaggregated and filtered in a 70-μm cell strainer in order to obtain a single-cell suspension. For confocal microscopy experiments 3 to 4 mice were pooled per condition and 10 mice were pooled for seahorse experiments. In these experiments, $CD8^+$ T lymphocytes from tumors and lymph nodes were magnetically isolated by using CD8 (Ly-2) MicroBeads positive selection (Miltenyi Biotec).

For tumor immunotherapy experiments, 5×10^5 B16-OVA cells were subcutaneously injected on day 0 in C57BL/6 or CD137KO mice. On day 3 or 5, OTI splenocytes were activated for 24 hours with 100 ng/mL of cognate SIINFEKL synthetic peptide and IL2 (50 IU/mL). After this 24 hours of culture, splenocytes were electroporated as explained below. Following a 16-hour culture for recovery, 2×10^6 T cells were intravenously transferred to the tumor-bearing mice (28, 29). B16-OVA tumors were measured with a precision caliper every 2 to 3 days.

DNA extraction and mitochondrial DNA PCR

DNA from costimulated human $CD8^+$ T lymphocytes was isolated using DNeasy Blood and Tissue kit (Sigma). The mitochondrial gene *mt-Co1* was measured by PCR carried out in a CFX real-time PCR detection system (BioRad) by using iQ SYBR green supermix (BioRad) and the following primer pair: forward 5′-GCTAGCCGCAGGCATTACTATAC-3′; reverse 5′-GCGGGATCAAAGAAAGTTGTG-3′. The levels of *mt-Co1* were normalized with the genomic gene *Hprt* (primer pair: forward 5′-TGGGAGGCCATCACATTGT-3′; reverse 5′-TCCAGCAGGTCAGCAAAGAA-3′) and represented according to this formula $2^{\Delta Ct\ (Ct\ Hprt\ -\ Ct\ mt\text{-}Co1)}$, where Ct corresponds to cycle number.

Seahorse assays

Oxygen consumption rates (OCR) and extracellular acidification rates (ECAR) were measured in an XF24 Extracellular flux analyzer (Seahorse Biosciences). Three hundred thousand $CD8^+$ T lymphocytes were plated in each well in a media containing non-buffered DMEM with 50 mmol/L glucose, 4 mmol/L Na-Pyruvate, and 2 mmol/L glutamine (all from Sigma). OCR and ECAR were measured in baseline conditions and in the presence of 0.5 μmol/L oligomycin, 1 μmol/L CCCP, 1 μmol/L antimycin A, and 1 μmol/L rotenone (All from Sigma). In some experiments, etomoxir (100 μmol/L) or DMSO, as control, were used after CCCP.

siRNA transfections

Purified CD8 T lymphocytes were activated with plate-bound anti-CD3ε (1 μg/mL, clone 145-2C11, BioLegend) for 4 hours and transfected with 200 pmol per 10^6 cells of human OPA-1 (AAGUUAUCAGUCUGAGCCAGGUU; AACCUGGCUCAGACUGAUACUU), mouse OPA-1 (GCCGAGGAUAGCUUGAGGGUUAU, AUAACCCUCAAGCUAUCCUGGC) MFN 1 (GGUCGCAAACUCUGAAUCAACAC, GUGUUGAUUCAGAGUUUGCGACC), and MFN2 (UGGACAGCUGGAUUGACAAGUUU, AAACUUGUCAAUCCAGCUGUCCA) targeting siRNA or control siRNA using a Gene pulser Mx System (BioRad). One hour following transfection, T lymphocytes were costimulated with plate-bound anti-CD3 (0.5 μg/mL, clone 145-2C11, BioLegend) and anti-CD137 (10 μg/mL, clone 1D8) for 72 hours or were adoptively transferred to tumor-bearing mice.

In vitro cytotoxicity assays

In vitro cytotoxicity assays were performed by measuring electric impedance in an Excelligence machine (ACEA). OTI splenocytes were activated overnight with SIINFEKL peptide and then OPA-1 or CTRL siRNA was electroporated. After resting for 2 hours, cells were seeded onto plates with plate-bound anti-CD3 and anti-CD137 or IgG and cultured for 72 hours. Cells were then collected and seeded in IL7 (25 ng/mL) supplemented media for additional 4 days. Then, 20,000 B16-OVA cells well seeded on special 8-well plates to measure electric impedance. After 3 hours, 200,000 OTI cells were added per well in triplicates. Electric impedance was measured every 5 minutes for additional 24 hours.

OPA-1 immunoblot

$CD8^+$ T cells were lysed at 4°C in RIPA lysis buffer. Proteins were quantified by BCA (Pierce) eluted in Laemmli buffer, separated by SDS–PAGE, and transferred to polyvinylidene difluoride membranes (Millipore). Membranes were blocked in TBS containing 0.05% Tween-20 and 10% nonfat milk for 1 hour. Immunoblots were performed with the mouse anti-hOPA-1 (BD Bioscience). Anti–β-Actin (clone AC-74; Sigma-Aldrich) was used as a loading control. Blots were developed with the SuperSignal West Dura Extended Duration Substrate (Pierce).

Isolation and culture of human TILs

TILs were obtained by processing ovarian and renal carcinoma biopsies with a Gentle Macs dissociator (Miltenyi). After two consecutive Ficoll gradient steps, the isolated leukocytes were costimulated in 96-well plates coated with anti-CD3ε (0.5 μg/mL; clone OKT3) and anti-CD137 (10 μg/mL; clone 6B4) for 72 hours.

Statistical analysis

Differences in metabolic and mitochondria parameters, tumor growth, and gene and protein expression were analyzed with Prism software (GraphPad Software). For comparisons, when results fit normality, Student *t* tests were used and Mann–Whitney *U* tests were used otherwise. For paired samples, Student *t* tests for paired samples were used. *P* values are indicated in figures.

Results

CD137 costimulation boosts mitochondrial size and membrane potential

Human and mouse T-cell cultures under CD137 costimulation acquire a more blastic morphology and more rapidly acidify the culture medium than their non-costimulated counterparts. Because these changes are indicative of more glycolysis, we explored whether agonistic anti-CD137 costimulation could also increase mitochondrial function. Treatment of human T-cell cultures with mAb to CD3ε, which mimics TCR signaling, resulted in enlarged mitochondria when cotreated with an agonistic mAb to CD137 (ref. 30; Fig. 1A and B). Moreover, when such T cells were examined by electron microscopy, a similar enlarged pattern following anti-CD137 costimulation (Fig. 1C and D) was observed. We studied whether mitochondrial changes were also induced by the physiological ligand, CD137L (31). Human $CD8^+$ T cells stimulated with anti-CD3ε in the presence of recombinant CD137L-coated microbeads also showed a 2-fold enlargement of their mitochondria (Fig. 1E). The effect of agonistic anti-CD137 was reproduced in spleen mouse $CD8^+$ T cells (Fig. 1F). Upon CD137 costimulation, both human and mouse $CD8^+$ T cells showed significantly enhanced mitochondrial mass revealed by MitoTracker staining and increased mitochondrial membrane potential (MMP) measured with a TMRM probe (Fig 1G and H).

To better understand which particular subset of costimulated $CD8^+$ T cells were exhibiting the most enlarged mitochondria, we decided to differentially sort $CD8^+$ T cells based on TMRM staining into high and low subsets. As previously reported (32), $TMRM^{Hi}$ cells acquired more surface CD25, but also more CD8 and showed larger size as measured by FSC (Supplementary Fig. S1A and S1B). The $TMRM^{Hi}$ subset of CD137-costimulated $CD8^+$ T lymphocytes exhibited the largest mitochondria (Supplementary Fig. S1C and S1D). Consistently, when confocal microscopy was used to analyze CD25 expression simultaneously with mitochondrial size, both parameters correlated ($R^2 = 0.295$; $P = 0.006$; Supplementary Fig. S1E and S1F). Higher transmembrane potential correlated with more proficient production of IFNγ (Supplementary Fig. S1G), suggesting more prominent effector functions. Moreover, FACS-sorted human peripheral blood $CD8^+$ T-cell subsets (Supplementary Figs. S2A and S2B) were studied for MitoTracker, TMRM staining, and mitochondrial size (Supplementary Fig. S2C and S2D) showing that CD137 costimulation increased such parameters in the three studied subsets (central memory, effector memory, and effector CD8 T cells), when separately costimulated in culture. When MitoTracker-high and -low cells were FACS-sorted, prestained with fluorescent dyes, remixed, and costimulated together, no differences were observed in the cell proportions contributing to the final outcome, suggesting that the effect of CD137 costimulation was not due to enrichment of a particular subset with high MitoTracker staining (Supplementary Fig. S2E). MitoTracker-high cells showed more intense expression of CD137 (Supplementary Fig. S2F). MitoTracker-low cells can be turned into MitoTracker-high cells by CD137 costimulation, pointing to a direct functional effect of CD137 ligation (Supplementary Fig. S2G and S2H). In addition, T cells do not selectively proliferate, as compared with naïve T cells (12), so that does not account for the mitochondrial effect in these costimulation cultures.

To address whether CD137 mitochondrial effects could be attributed to autocrine cytokines produced upon costimulation, we explored a potential effect of IL2 and IFNγ on mitochondrial parameters. Mitochondrial morphology, TMRM, or MitoTracker staining—upon neutralization or exogenous addition of such cytokines, either in the presence or absence of CD137 costimulation—was not significantly affected (Supplementary Fig. S3A–S3C). These results support a direct effect of CD137 costimulation in mitochondrial changes, although it remains to be determined whether other unidentified autocrine factors could contribute.

CD137 costimulation enhances mitochondrial respiratory capabilities in $CD8^+$ T cells

Time-lapse follow-up of baseline and maximal OCRs reflects the basal respiration and spare respiratory capacity [SRC, maximal OCR (MRR) – basal OCR(BRR)] of cells, whereas ECAR is indicative of glycolysis. In our experiments, human $CD8^+$ T cells showed more basal and maximal respiration and increased SRC and ECAR when costimulated with the mAb 6B4 to CD137 for 72 hours (Fig. 2A–C) and replicated with urelumab, the anti-CD137 that is used in phase II clinical trials for cancer (14). Similarly, CD137-costimulated $CD8^+$ T cells from mouse splenocytes

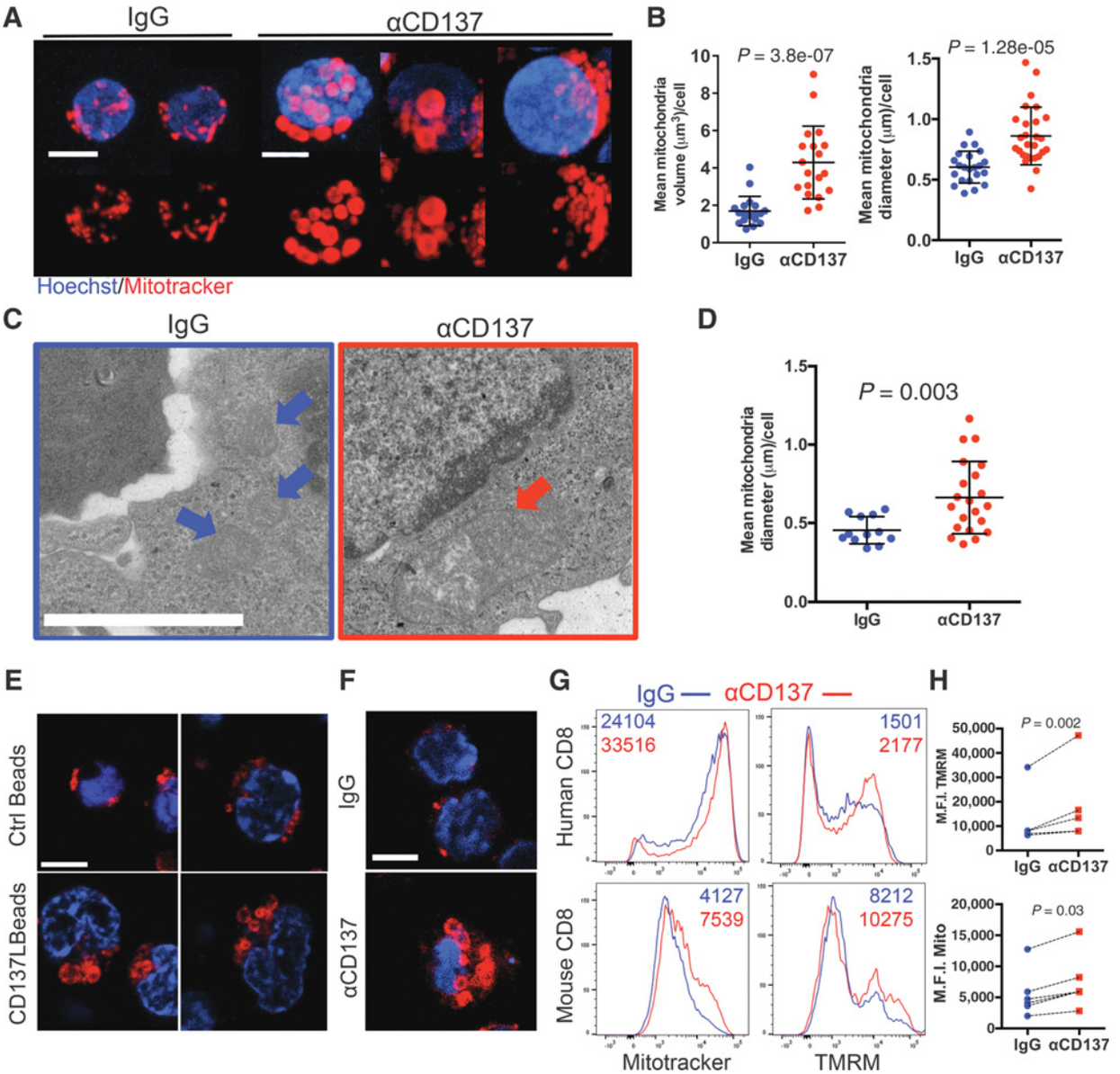

Figure 1.

CD137 costimulation induces mitochondrial enlargement and increases mitochondrial transmembrane potential in CD8 T cells. **A–G,** $CD8^+$ T cells were activated either with anti-CD3 and irrelevant IgG or anti-CD137 agonistic antibodies for 72 hours. **A,** Representative images (3D reconstruction of Z stacks) and (**B**) mean mitochondrial volume and diameter of individual human $CD8^+$ T cells. **C,** Representative transmission electron microscopy images of mitochondria in human $CD8^+$ T cells treated with CD137 agonistic antibodies as in **A** (bar, 2 μm). **D,** Mean mitochondrial diameter per cell measured on images as in **C**. **E,** Representative confocal images of mitochondria in human $CD8^+$ T cells activated with anti-CD3 and beads coated with CD137L or control protein. **F,** Representative confocal images of mitochondria in mouse $CD8^+$ T cells with or without CD137 costimulation by agonist 1D8 mAb. **G,** Representative FACS histograms of mouse and human CD8 T cells stained with MitoTracker to estimate mitochondrial mass and TMRM to measure mitochondrial transmembrane potential following CD137 costimulation (red) or controlled by IgG (blue). **H,** Coupled data of T cells from six independent healthy donors. Bars (5 μm). In **B** and **D**, each dot represents an individual cell. *P* values are shown, Mann–Whitney *U* test, and Wilcoxon paired test for **G**. All the data are representative of at least two experiments.

showed increases in basal and maximal respiration, SRC, and ECAR (Fig. 2D–F), confirmed these results in five independent experiments to account for individual OCR baseline variability (Fig. 2G–I). These results indicate that anti-CD137 costimulation boosts both mitochondrial respiration and glycolysis. SRC increased by CD137 costimulation was abolished by inhibition of CPT-1A with etomoxir (Supplementary Fig. S4A), suggesting the involvement of fatty acid oxidation in the CD137 enhanced respiratory function. In keeping with this observation, *CPT1A* mRNA expression was increased by CD137 costimulation in mouse and human $CD8^+$ T cells (Supplementary Fig. S4B and S4C).

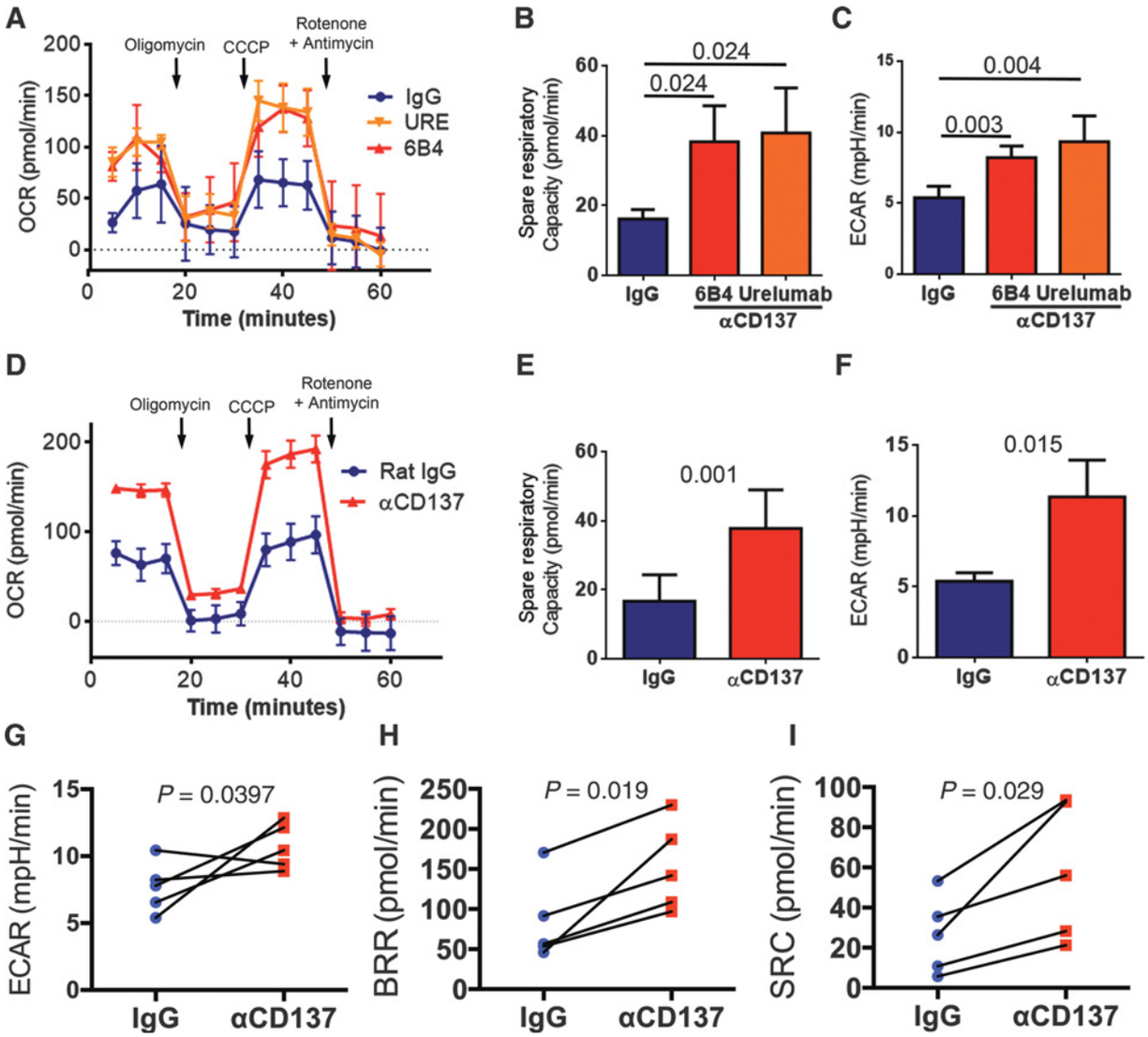

Figure 2.

Mitochondrial respiration is upregulated by CD137 costimulation. $CD8^+$ T cells (murine and human) were activated for 72 hours with anti-CD137 (red/orange) or IgG control (blue). Human $CD8^+$ T cells were stimulated either with 6B4 anti-CD137 agonistic antibody or with clinical grade anti-CD137 urelumab (URE). OCRs of human (**A**) and mouse (**D**) $CD8^+$ T cells baseline and in sequential response to oligomycin, CCCP, and rotenone + antimycin. SRC (**B** and **E**) and baseline ECAR (**C** and **F**) of human (**B** and **C**) and mouse (**E** and **F**) CD8 T cells. **G–I**, Five independent repetitions of experiments as in **D**. Mean ± SD is shown. Individual *P* values are shown for each comparison using Student *t* tests. A representative experiment out from at least two performed is shown. In **G** to **I**, *P* values were calculated with paired *t* tests.

When compared with their anti-CD28 costimulated counterparts, anti-CD137 costimulated $CD8^+$ T cells showed enhanced basal and maximal respiration rates, increased SRC, but a similar ECAR (Fig. 3A–C). This could reflect an advantage of CD137 in inducing mitochondrial respiration, in addition to glycolysis. This is consistent with previous observations comparing the cytoplasmic tails of CD28 and CD137 in CARs (19). CD28 plus CD137 dual costimulation further increased MitoTracker content (Fig. 3D) and slightly enhanced mitochondrial size (Fig. 3E–G). Notably, concomitant costimulation via CD28 and CD137 resulted in additive effects on respiratory capacity (Fig. 3).

OPA-1 dependency of CD137 effects on mitochondria

In addition to the mitochondrial hypertrophy found after CD137 costimulation (Fig. 1), our seahorse results would also be explained by an increased number of mitochondria. Quantification experiments did not reveal any detectable increase in the number of mitochondria (Fig. 3G), suggesting that the main effect of anti-CD137 treatment was the generation of enlarged mitochondria. Mitochondrial DNA content relative to nuclear DNA did not significantly change after CD137 costimulation, which further supported a similar absolute number of mitochondria (Supplementary Fig. S5A).

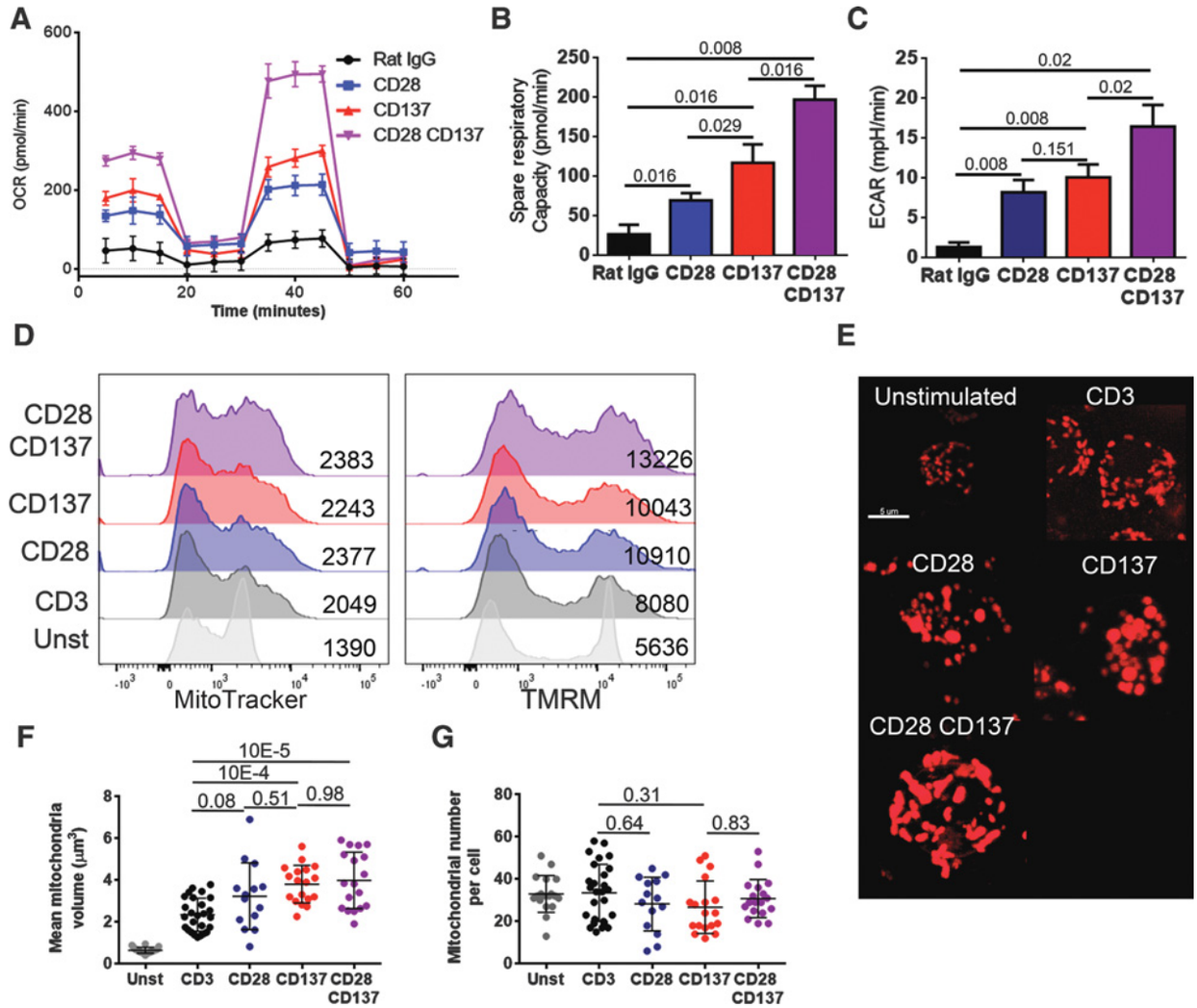

Figure 3.

CD137 is superior to CD28 at promoting mitochondrial enlargement and respiration. **A–G**, $CD8^+$ T cells were costimulated with agonistic antibodies against CD3 and CD137, CD28, CD137 plus CD28, or IgG control for 72 hours or left unstimulated with IL7 for these 72 hours. OCR (**A**), SRC (**B**), and ECAR (**C**) of mouse CD8 T cells in response to oligomycin, CCCP, and rotenone + antimycin were determined. **D,** Representative FACS histograms of mitochondrial mass (MitoTracker) and TMRM of human $CD8^+$ T cells. **E,** Representative confocal images (3D reconstruction of Z stacks) of human $CD8^+$ T cells treated with agonistic antibodies. Mean mitochondrial volume (**F**) and number of mitochondria in individual human $CD8^+$ T cells (**G**) (dots represent individual cells). Mean ± SD. For statistical comparison *P* values are shown. Mann–Whitney *U* tests applied. Representative data of two experiments are shown.

The expression of genes involved in mitochondrial dynamics (33) was similar after anti-CD137 costimulation, although slight increases were noted in genes controlling mitochondrial biogenesis and fusion (Supplementary Fig. S5B–S5D). Expression of these genes involved in mitochondrial biogenesis and fusion was greater with dual CD137 + CD28 costimulation over CD28 single-agent costimulation (Supplementary Fig. S5E and S5F). This suggests nonredundant roles of CD137 and CD28 in this regard.

The protein OPA-1 (optic atrophy-1) is involved in the remodeling and fusion of mitochondrial inner membrane cristae (23, 34). We observed increased OPA-1 protein expression by flow cytometry after CD137 costimulation (Fig. 4A) and by immunoblot (Supplementary Fig. S5G and S5H). To test whether the expression of OPA-1 was required for the effect of agonist anti-CD137 in enhancing mitochondrial mass and MMP, we electroporated human $CD8^+$ T cells with control or OPA-1 siRNA. Silencing of OPA-1 was confirmed by qRT-PCR over 120 hours and did not affect proliferation or apoptosis in the $CD8^+$ T-cell cultures (Supplementary Fig. S6). However, OPA-1 silencing did impair effector functions such as production of IFNγ and TNFα and *in vitro* cytotoxicity (Supplementary Fig. S6E and S6F). Mitochondrial enlargement and MMP were significantly reduced in response to anti-CD137, to levels comparable to isotype control-treated human $CD8^+$ T cells (Fig. 4B–D). In addition, increased baseline and maximal respiration, SRC, and ECAR following anti-CD137 treatment was also blocked by OPA-1 siRNA (Fig. 4E and F). The enhanced surface expression of CD25

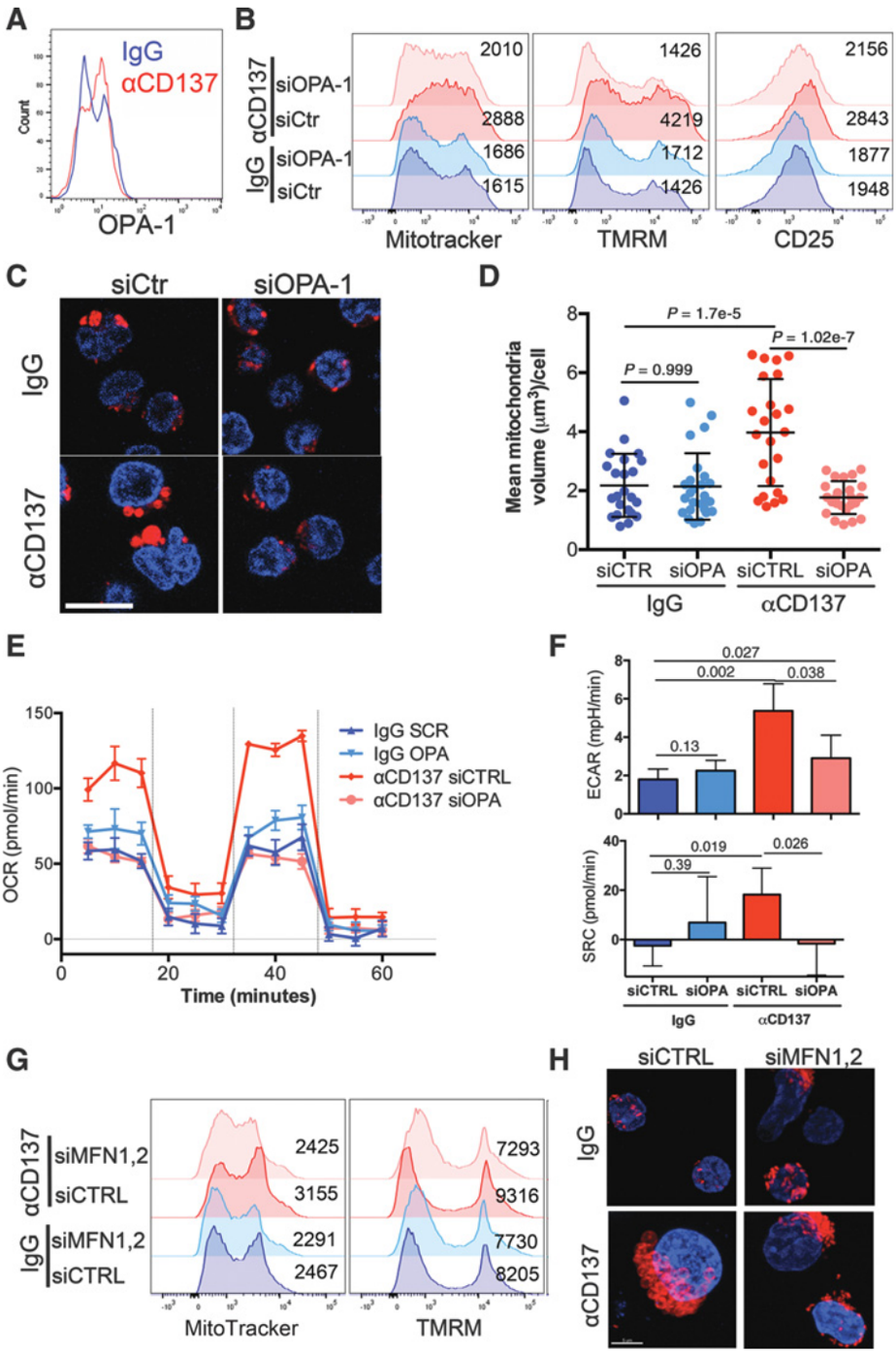

Figure 4.

Mitochondrial remodeling induced by CD137 costimulation is dependent on OPA-1 protein. **A,** Representative FACS histograms of OPA-1 intracellular staining on CD8 T cells activated with CD137 agonistic antibodies or IgG control for 72 hours. CD8 T cells were electroporated with a siRNA targeting OPA-1 and then activated for 72 hours in culture with anti-CD137 or isotype control. **B,** Representative FACS histograms of mitochondrial mass per cell (MitoTracker), mitochondrial transmembrane potential (TMRM), and surface CD25 on human CD8 T cells. Confocal microscopy images of mitochondria (**C**) and quantification of mitochondrial volume (**D**) on OPA-1 siRNA or control siRNA-transfected human CD8 T cells. **E** and **F,** OCR, ECAR, and SRC of OPA-1 siRNA-transfected CD8 T cells in the sequential presence of oligomycin, CCCP, and antimycin + rotenone (as in Fig. 2). **G** and **H,** Human $CD8^+$ T cells were electroporated with siRNA against MFN1 and MFN2 or control siRNA and then activated for 72 hours with anti-CD137 or isotype control. **G,** Representative FACS histograms of mitochondrial mass (MitoTracker), TMRM, and surface CD25 on human CD8 T cells. **H,** Confocal images of mitochondria MFN1 and MFN2 siRNA-transfected human CD8 T cells. Representative data from at least two experiments are shown.

induced by CD137 costimulation was reduced by OPA-1 siRNA (Fig. 4B). Consistent with these findings, siRNA silencing of mitofusin 1 and 2 proteins, involved in the fusion of the mitochondrial outer membrane (23, 34), rendered comparable results (Fig. 4G and H).

Overall, these data suggest that mitochondrial fusion proteins are needed for the effect of anti-CD137 in mitochondrial morphology and MMP in $CD8^+$ T cells. The train of events between CD137 biochemical signals and mitochondrial response remain to be elucidated but published evidence suggests the Akt–mTOR pathway as a likely candidate (35). In keeping with this concept, we observed an increase of phosphorylated S6 upon CD137 costimulation that was not inhibited by siOPA-1 (Supplementary Fig. S7A–S7C), suggesting that OPA-1 operates downstream of mTOR. We could not test directly the effect of mTOR inhibitors, because they strongly downregulated CD3 activation in the cultures. Notably, the AKT inhibitor MK-2206 impaired CD137-dependent increase in the mitochondrial

mass and transmembrane potential without noticeable effect on CD25 upregulation (Supplementary Fig. S7D–S7F). These data suggest that both mTOR and AKT are involved in the mitochondrial changes induced by CD137 costimulation, seemingly acting upstream of OPA-1.

Mitochondrial effects of CD137 costimulation in cancer-bearing mice

CD137 costimulation is currently exploited for cancer immunotherapy (6, 13, 36). Mitochondria in tumor-infiltrating T lymphocytes (TIL) are compromised in function and mass (24). We thus explored the involvement of endogenous CD137–CD137L interactions in regulating mitochondrial morphology and function in tumor-reactive T cells in tumor-bearing mice. MC38-derived tumors were engrafted in $CD137^{-/-}$ and WT syngeneic mice. $CD8^+$ TILs and $CD8^+$ T cells from TDLN showed reduced mitochondrial mass and MMP when the tumors developed in CD137-deficient mice (Fig. 5A and B). Such changes were not observed in T lymphocytes located in the TDLNs from the contralateral side. $CD8^+$ T cells in TDLN of $CD137^{-/-}$ mice showed reduced basal and maximal respiration rates (Fig. 5C) and similar ECAR. Absolute numbers of $CD137^{-/-}$ $CD8^+$ T cells were not significantly reduced in the microenvironment of MC38 tumors (Supplementary Fig. S8A and S8B). FACS analyses of MitoTracker staining in TDLN showed clear reduction in the $CD137^{-/-}$ compartment (Supplementary Fig. S8C and S8D). Differentially gating $PD\text{-}1^+$ and $PD1^+Ki67^+$ cells, these differences were also substantiated indicating that tumor-reactive $CD137^{-/-}$ also showed reduced mitochondrial parameters (Supplementary Fig. S8D).

CD137 and CD28 costimulation did not have redundant roles in driving mitochondrial enlargement and respiratory functions (Fig. 3). CD28 can costimulate $CD137^{-/-}$ $CD8^+$ T cells to increase their respiratory capacity (Supplementary Fig. S8E). However, the increase elicited by CD28 costimulation was lower in $CD137^{-/-}$ CD8 T cells than in WT counterparts, suggesting a role for endogenous CD137/CD137L functions (Supplementary Fig. S8F), consistent with the described increase in expression of CD137L on T cells upon activation (37). In this regard, blockade with anti-CD137L also reduced baseline and maximal respiratory capacity upon CD28 costimulation (Supplementary Fig. S8G).

We then tested the effects of CD137 mAbs in B16-OVA melanoma–bearing mice, transferring WT or $CD137^{-/-}$ TCR-transgenic OVA-specific OT-I $CD8^+$ T cells and concomitantly treated such mice with agonist anti-CD137 or control antibody. Mitochondria in OT-I $CD8^+$ T cells from TDLN became enlarged as detected by MitoTracker staining assessed by flow cytometry (Fig. 6A and B) and confocal microscopy (Fig. 6F). This effect was dependent on CD137, as it was not observed when CD137-deficient OTI $CD8^+$ T cells were transferred (Fig. 6G). Consistently, basal and maximal respiration rates, SRC and ECAR were also increased in OT-I $CD8^+$ T cells from the TDLNs (Fig. 6C–E).

To extend these data to TILs, $CD8^+$ T cells were recovered from B16-OVA tumors treated as above. In this case, $CD8^+$ T cells also had enhanced mitochondrial respiration when mice had received anti-CD137 (Supplementary Fig. S9A). Anti-CD137 costimulation of anti-CD3-stimulated human TILs from three independent tumor surgical specimens (two ovary adenocarcinomas and one clear-cell renal cell carcinoma) resulted in increased mitochondrial size and MMP, compared with costimulation with an isotype matched control antibody (Supplementary Fig. S9B and S9C).

The fate of adoptively transferred cells was followed for 10 days to understand the effects of OPA-1 silencing upon CD137 costimulation. No noticeable effects in recovered cell numbers or changes in KLRG1 expression (indicating effector differentiation) were found in OPA-1–silenced cells either in the tumor or TDLN (Supplementary Figs. S10B and S10C). OPA-1 partial silencing only resulted in a discrete augmentation in CD62L cells and fewer $EOMES^+$ cells (Supplementary Figs. S10D–S10F), perhaps indicating subtle changes toward memory differentiation.

To ascertain whether OPA-1–mediated mitochondrial function enhancement was required for anti-CD137 agonist immunotherapeutic effects, we adoptively transferred OPA-1–silenced OTI T cells (electroporated with OPA-1 or control siRNA) to B16-OVA tumor-bearing $CD137^{-/-}$ mice (Fig. 7A and B). A single dose of agonistic anti-CD137 or control antibody was given in combination. We observed that only the siCTRL-transfected OTI T cells combined with anti-CD137 were able to induce regression of B16-OVA tumors, suggesting that OPA-1 protein was needed for key CD137 immunotherapy functions on anti-tumor T lymphocytes.

Discussion

In this study, we unravel a functional connection between CD137 costimulation and enhanced size and metabolic functions in T-cell mitochondria. Mitochondria enlargement is the most prominent feature observed by confocal and electron microscopy upon CD137 costimulation. Previous observations with the CD137 cytoplasmic tail built into anti-CD19 chimeric antigen receptors (19) suggested prominent effects of CD137 on mitochondria. However, CD3ζ placed in tandem in such constructions made it very difficult to ascertain if these functions were the result of the artificial chimeric molecules or an effect mediated by the naturally occurring moieties. Our results show that CD17 stimulation of primary human and mouse CD8 T lymphocytes with agonist antibodies or with the natural ligand results in enlarged mitochondria endowed with stronger respiratory capabilities.

The CD137 signaling events that lead to these effects on mitochondria need elucidation. Our results indicate a role for the AKT–mTOR route, whose function is upregulated by CD137 stimulation (38, 39). Yet, the mechanistic connection of CD137 crosslinking to such downstream events needs to be linked to the proximal signaling events at the CD137–TRAF2–TRAF-1 complexes (30, 40). Our results rule out a critical dependency on autocrine IL2 or IFNγ for CD137-induced mitochondrial invigoration, but other soluble mediators might be involved.

The effects we saw of CD137 stimulation on mitochondria were more intense than those elicited by CD28 (41), in terms of size and transmembrane potential. Concurrent CD137 and CD28 costimulation had additive effects on mitochondria. This could be merely a consequence of the enhanced CD137 expression that results from CD28 costimulation (42) or the result of functional cross-talk between the two costimulatory receptors. PD-1 blockade can also enhance mitochondrial function in T cells (25), perhaps as a result of releasing CD28 signaling toward PI3-kinase (43). In our hands, CD137-deficiency impairs CD28 costimulation of mitochondrial function parameters. This result in our costimulation cultures is most likely related to the

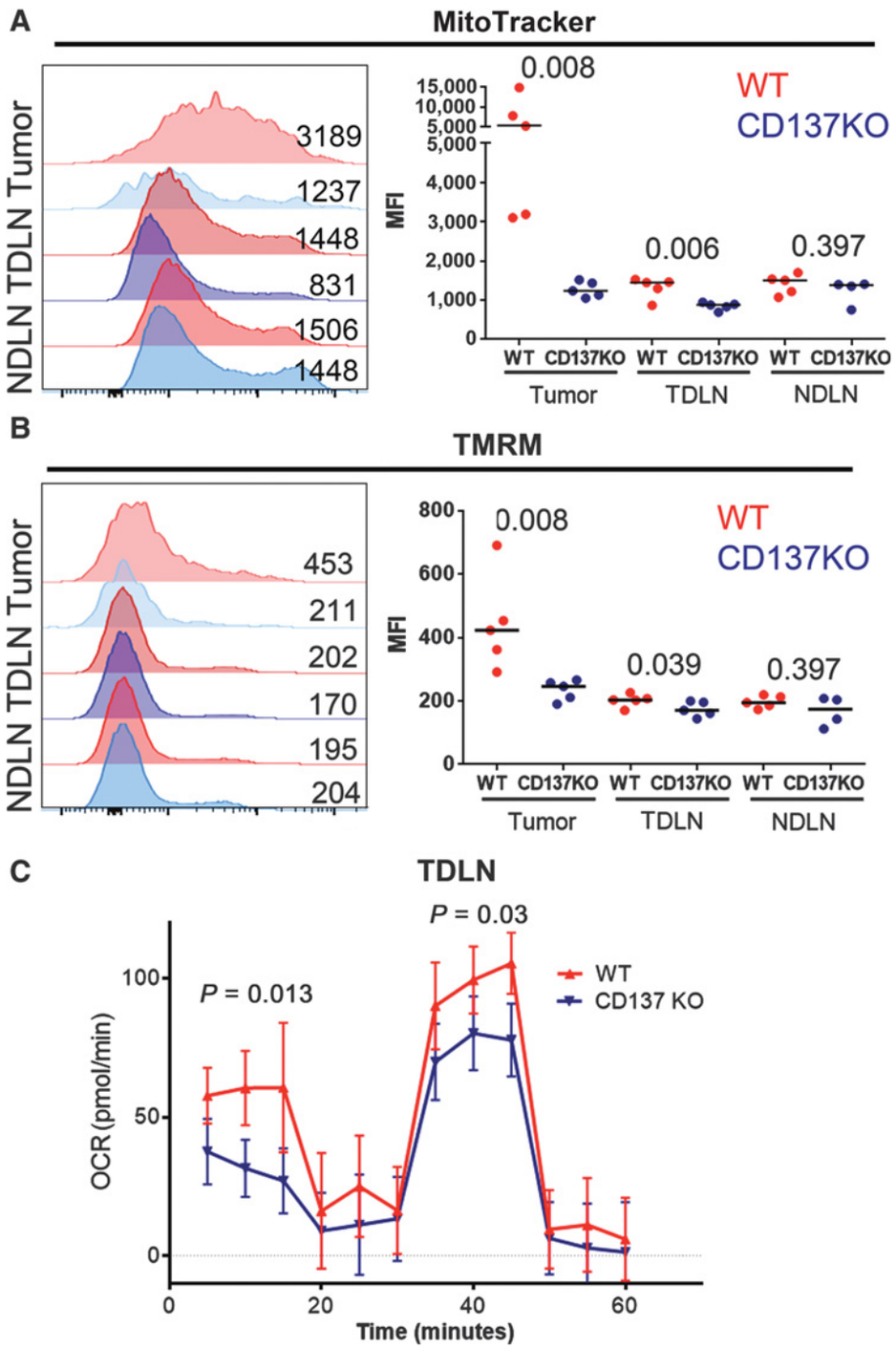

Figure 5.

CD137 controls mitochondrial mass and function in tumor-reactive CD8 T cells. **A–C,** MC38 derived tumors were s.c. engrafted on WT or CD137KO mice. Ten days later tumors, tumor-draining lymph nodes (DLN) or contralateral nondraining LNs were harvested. **A** and **B,** Representative FACS histograms and summary data of mitochondrial mass (MitoTracker; **A**) and mitochondrial transmembrane potential (TMRM; **B**) in $CD8^+$ T cells of the indicated tissue sources. **C,** $CD8^+$ T cells were magnetically isolated from tumor-draining lymph nodes (TDLN) of MC38-bearing WT or CD137KO mice. OCR was measured upon sequential addition of oligomycin, CCCP, and antimycin + rotenone. These experiments are representative of at least two experiments. Statistical comparisons were made by using the Student *t* test. Representative data from at least two similar experiments performed are shown.

endogenous interactions of CD137L that is reportedly induced on T cells (37). *In vivo* CD137L is probably also at play, explaining the baseline reduction in mitochondrial parameters observed in $CD137^{-/-}$ T cells.

CD137 exerts other metabolic effects aside from mitochondria functions, including an increase in anaerobic glycolysis (16), as also suggested by our ECAR observations in seahorse experiments. In this regard, a CD137-containing CAR did not increase glycolysis (19), perhaps suggesting differences between the chimeric and naturally occurring molecules.

It will be interesting to see if our results can be extended to other costimulatory receptors of the TNFR family, such as OX40, CD27, or GITR (44), and to compare these receptors for the intensity of such mitochondrial effects. T-cell exposure to IL15 can also have prominent effects on mitochondria (45), and it is tempting to speculate that many agents with activity in cancer

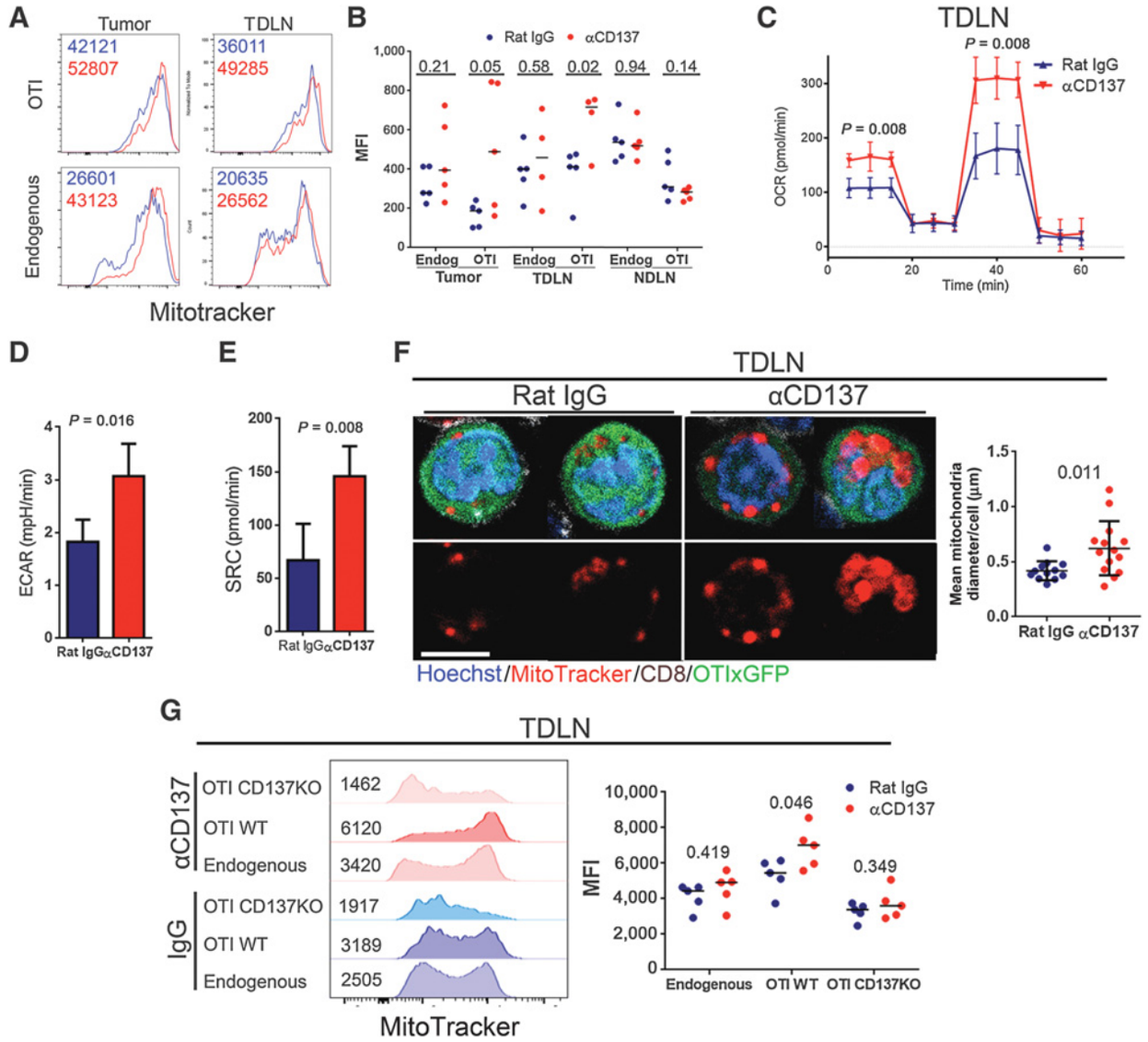

Figure 6.

Agonist CD137 antibodies increase mitochondrial fitness in tumor-reactive CD8 T lymphocytes. **A–F,** B16-OVA melanoma–bearing mice were adoptively transferred with splenocytes from OTIxGFP (and OTIxCD45.1xCD137KO mice in **G**) and simultaneously treated with agonistic anti-CD137 or rat IgG control. Three days later tumors, tumor-draining lymph nodes (TDLN) or NDLNs were harvested. In **A, C, D, E,** and **F**, $CD8^+$ T cells were magnetically purified. Representative FACS histograms (**A**) and summary data (**B**) of mitochondrial mass (MitoTracker) of OTI-transferred CD8 T cells or endogenous $CD8^+$ T cells in tumor and LNs of B16-OVA–bearing mice upon anti-CD137 treatment are shown. OCR (**C**), ECAR (**D**), and SRC (**E**) of $CD8^+$ T cells purified from TDLNs of B16-OVA–bearing mice treated with anti-CD137. **F,** Confocal microscopy of mitochondria on transferred OTI T cells upon treatment with anti-CD137 or IgG control. Representative images and quantification of the mean mitochondrial diameter per cell are shown. **G,** Representative FACS histograms and compiled data of mitochondrial mass (MitoTracker) assessed in OTI and OTI CD137KO adoptively transferred $CD8^+$ T cells or endogenous $CD8^+$ T cells in recovered TDLNs of B16-OVA–bearing mice upon anti-CD137 treatment. Medians and means ± SD are provided. Individual *P* values are shown. Statistical comparisons were made by using Student *t* tests. Representative data from at least two similar experiments performed are shown.

immunotherapy may share these invigorating effects on mitochondria. Cumulative experimental evidence points to mitochondrial dysfunction of T cells in the tumor microenvironment (46), suggesting opportunity for interventions with metabolic drugs such as metformin (47).

Various lines of evidence indicate a prominent role for OPA-1 in the CD137-induced effects, consistent with mitochondrial fusion and cristae remodeling (33). OPA-1 upregulation is likely the result of mTOR activity (48). We do not exclude a role for mitochondrial biogenesis in a concerted fashion with mitochondrial fusion (24). Indeed, we observe upregulated expression of several genes involved in mitochondrial biogenesis. Given the functions of OPA-1 on cristae remodeling and tightening, these effects are likely behind the functional augmentation of transmembrane potential and respiratory capabilities (23). It would be interesting to know if OPA-1 transgenic overexpression accounts

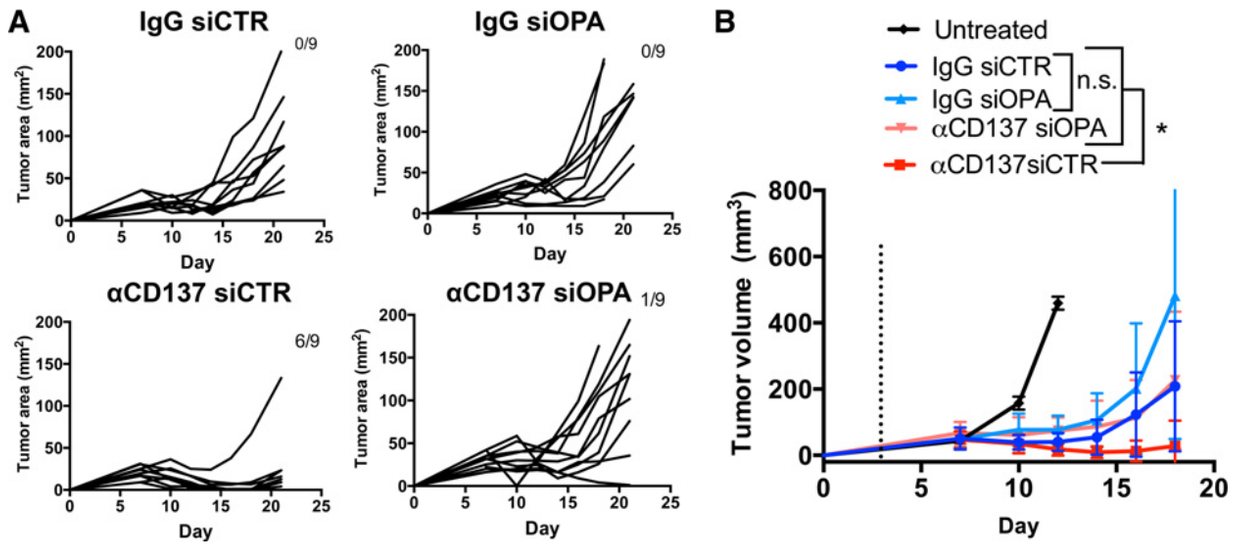

Figure 7.

OPA-1 silencing in OT-1 lymphocytes impairs their antitumor activity when combined to anti-CD137 treatment. OTI splenocytes were activated with SIINFEKL peptide and 50 U/mL IL2 for 24 hours, then lymphocytes were electroporated with OPA-1 or ctrl siRNA, and 2×10^6 cells were i.v. transferred to B16-OVA tumor–bearing CD137$^{-/-}$ mice on day +3. Individual follow-up of tumor sizes (area) is provided in **A**. In **B,** mean tumor volumes ± SD followed over time are shown ($n = 9$ per group). The experiment is representative from two similarly performed and rendered similar results when performed in WT mice instead of CD137KO mice (Supplementary Fig. S10A). *, $P < 0.05$, Mann–Whitney *U* test.

for all the mitochondrial changes observed upon CD137 costimulation.

In addition to metabolic functions, mitochondria play key roles in apoptosis and its regulation. Hyperpolarized and enlarged mitochondria resulting from CD137 costimulation might behave differently and perhaps participate in the inhibition of T-cell apoptosis in conjunction with BCL-x_L upregulation by CD137 (38).

Dysfunctional and exhausted tumor-infiltrating T cells (49) express CD137 (20). If tumor-reactive TILs were deficient in CD137, their mitochondria mass and functional capabilities would be hindered. We observe invigoration of mitochondrial mass and function upon therapy with anti-CD137 in mice and parallel effects are observed in human lymphocytes cultured from the tumor microenvironment. Of note, it has been reported that addition of CD137 to TIL cultures increases the yield and performance of the resulting T cells (50).

In conclusion, mitochondria are the power plants for energy generation (51) and the metabolic factories to supply biomolecules for T-cell division and function (1). Our findings indicate that CD137 costimulation upregulates such functions with important implications for cancer immunotherapy. Particularly, CD137-based costimulation may be of great use to reinvigorate endogenous antitumor T cells for adoptive transfer–based T-cell therapies (28, 29, 50). Monitoring mitochondrial parameters could also result in much needed pharmacodynamic biomarkers for CD137-based immunotherapy strategies under clinical development (11).

Disclosure of Potential Conflicts of Interest

I. Melero reports receiving commercial research grants from Alligator, Bristol-Myers Squibb, and Roche; has received speakers bureau honoraria from MSD; and is a consultant/advisory board member for Bristol-Myers Squibb, Roche, Merck-Serono, Tusk, Genmab, and Bayer. No potential conflicts of interest were disclosed by the other authors.

Authors' Contributions

Conception and design: A. Teijeira, S. Labiano, I. Melero
Development of methodology: S. Labiano, E. Santamaría, M. Enamorado, I. Melero
Acquisition of data (provided animals, acquired and managed patients, provided facilities, etc.): A. Teijeira, S. Labiano, I. Etxeberria, E. Santamaría, M. Enamorado, A. Azpilikueta, S. Inoges, E. Bolaños, A.R. Sánchez-Paulete
Analysis and interpretation of data (e.g., statistical analysis, biostatistics, computational analysis): A. Teijeira, S. Labiano, A. Rouzaut, M.A. Aznar, D. Sancho, I. Melero
Writing, review, and/or revision of the manuscript: A. Teijeira, S. Labiano, I. Etxeberria, M. Enamorado, S. Inoges, M.A. Aznar, D. Sancho, I. Melero
Administrative, technical, or material support (i.e., reporting or organizing data, constructing databases): S. Garasa, A. Azpilikueta
Study supervision: I. Melero

Acknowledgments

This project was supported by imCORE Network (Roche Genentech), MINECO (SAF2014-52361-R, 2017-83267-C2-1-R; I. Melero), European Commission VII Framework and Horizon 2020 programs (IACT and PROCROP), Fundación de la Asociación Española Contra el Cáncer (AECC), and Fundación BBVA. A. Teijeira receives support from a Juan de la Cierva contract, MINECO.

Electron and light microscopy CIMA services as well as Flow Cytometry CIMA facilities (Diego Alignani) and personnel at blood bank of Navarra are acknowledged for their technical support. We are also grateful to Drs. Lasarte and Hervas-Stubbs for scientific discussion and to Dr. Paul Miller for editing the manuscript.

The costs of publication of this article were defrayed in part by the payment of page charges. This article must therefore be hereby marked *advertisement* in accordance with 18 U.S.C. Section 1734 solely to indicate this fact.

Received December 29, 2017; revised March 23, 2018; accepted April 19, 2018; published first April 20, 2018.

References

1. Chang CH, Qiu J, O'Sullivan D, Buck MD, Noguchi T, Curtis JD, et al. Metabolic competition in the tumor microenvironment is a driver of cancer progression. Cell 2015;162:1229–41.
2. O'Neill LA, Kishton RJ, Rathmell J. A guide to immunometabolism for immunologists. Nat Rev Immunol 2016;16:553–65.
3. Ho PC, Bihuniak JD, Macintyre AN, Staron M, Liu X, Amezquita R, et al. Phosphoenolpyruvate is a metabolic checkpoint of anti-tumor T cell responses. Cell 2015;162:1217–28.
4. Chen L, Flies DB. Molecular mechanisms of T cell co-stimulation and co-inhibition. Nat Rev Immunol 2013;13:227–42.
5. Frauwirth KA, Riley JL, Harris MH, Parry RV, Rathmell JC, Plas DR, et al. The CD28 signaling pathway regulates glucose metabolism. Immunity 2002;16:769–77.
6. Sanchez-Paulete AR, Labiano S, Rodriguez-Ruiz ME, Azpilikueta A, Etxeberria I, Bolanos E, et al. Deciphering CD137 (4–1BB) signaling in T-cell costimulation for translation into successful cancer immunotherapy. Eur J Immunol 2016;46:513–22.
7. Kwon BS, Hurtado JC, Lee ZH, Kwack KB, Seo SK, Choi BK, et al. Immune responses in 4–1BB (CD137)-deficient mice. J Immunol 2002;168: 5483–90.
8. McNamara JO, Kolonias D, Pastor F, Mittler RS, Chen L, Giangrande PH, et al. Multivalent 4–1BB binding aptamers costimulate CD8+ T cells and inhibit tumor growth in mice. J Clin Invest 2008;118:376–86.
9. Bartkowiak T, Curran MA. 4–1BB agonists: multi-potent potentiators of tumor immunity. Front Oncol 2015;5:117.
10. Xu DP, Sauter BV, Huang TG, Meseck M, Woo SL, Chen SH. The systemic administration of Ig-4–1BB ligand in combination with IL-12 gene transfer eradicates hepatic colon carcinoma. Gene Ther 2005;12:1526–33.
11. Chester C, Sanmamed MF, Wang J, Melero I. Immunotherapy targeting 4–1BB: mechanistic rationale, clinical results, and future strategies. Blood 2018;131:49–57.
12. Aznar MA, Labiano S, Diaz-Lagares A, Molina C, Garasa S, Azpilikueta A, et al. CD137 (4–1BB) costimulation modifies DNA methylation in CD8(+) T cell-relevant genes. Cancer Immunol Res 2018;6:69–78.
13. Ascierto PA, Simeone E, Sznol M, Fu YX, Melero I. Clinical experiences with anti-CD137 and anti-PD1 therapeutic antibodies. Semin Oncol 2010; 37:508–16.
14. Segal NH, Logan TF, Hodi FS, McDermott D, Melero I, Hamid O, et al. Results from an integrated safety analysis of urelumab, an agonist anti-CD137 monoclonal antibody. Clin Cancer Res 2017;23:1929–36.
15. Fisher TS, Kamperschroer C, Oliphant T, Love VA, Lira PD, Doyonnas R, et al. Targeting of 4–1BB by monoclonal antibody PF-05082566 enhances T-cell function and promotes anti-tumor activity. Cancer Immunol Immunothera 2012;61:1721–33.
16. Choi BK, Lee DY, Lee DG, Kim YH, Kim SH, Oh HS, et al. 4–1BB signaling activates glucose and fatty acid metabolism to enhance $CD8^+$ T cell proliferation. Cell Mol Immunol 2017;14:748–57.
17. Carpenito C, Milone MC, Hassan R, Simonet JC, Lakhal M, Suhoski MM, et al. Control of large, established tumor xenografts with genetically retargeted human T cells containing CD28 and CD137 domains. PNAS 2009;106:3360–5.
18. Fesnak AD, June CH, Levine BL. Engineered T cells: the promise and challenges of cancer immunotherapy. Nat Rev Cancer 2016;16:566–81.
19. Kawalekar OU, O'Connor RS, Fraietta JA, Guo L, McGettigan SE, Posey AD Jr, et al. Distinct signaling of coreceptors regulates specific metabolism pathways and impacts memory development in CAR T cells. Immunity 2016;44:380–90.
20. Williams JB, Horton BL, Zheng Y, Duan Y, Powell JD, Gajewski TF. The EGR2 targets LAG-3 and 4–1BB describe and regulate dysfunctional antigen-specific CD8+ T cells in the tumor microenvironment. J Exp Med 2017;214:381–400.
21. Bengsch B, Johnson AL, Kurachi M, Odorizzi PM, Pauken KE, Attanasio J, et al. Bioenergetic insufficiencies due to metabolic alterations regulated by the inhibitory receptor PD-1 are an early driver of CD8(+) T cell exhaustion. Immunity 2016;45:358–73.
22. Champagne DP, Hatle KM, Fortner KA, D'Alessandro A, Thornton TM, Yang R, et al. Fine-tuning of CD8(+) T cell mitochondrial metabolism by the respiratory chain repressor MCJ dictates protection to influenza virus. Immunity 2016;44:1299–311.
23. Buck MD, O'Sullivan D, Klein Geltink RI, Curtis JD, Chang CH, Sanin DE, et al. Mitochondrial dynamics controls T cell fate through metabolic programming. Cell 2016;166:63–76.
24. Scharping NE, Menk AV, Moreci RS, Whetstone RD, Dadey RE, Watkins SC, et al. The tumor microenvironment represses T cell mitochondrial biogenesis to drive intratumoral T cell metabolic insufficiency and dysfunction. Immunity 2016;45:374–88.
25. Chamoto K, Chowdhury PS, Kumar A, Sonomura K, Matsuda F, Fagarasan S, et al. Mitochondrial activation chemicals synergize with surface receptor PD-1 blockade for T cell-dependent antitumor activity. PNAS 2017;114: E761–E70.
26. Sukumar M, Liu J, Ji Y, Subramanian M, Crompton JG, Yu Z, et al. Inhibiting glycolytic metabolism enhances CD8+ T cell memory and antitumor function. J Clin Invest 2013;123:4479–88.
27. Teijeira A, Palazon A, Garasa S, Marre D, Auba C, Rogel A, et al. CD137 on inflamed lymphatic endothelial cells enhances CCL21-guided migration of dendritic cells. FASEB J 2012;26:3380–92.
28. Weigelin B, Bolanos E, Rodriguez-Ruiz ME, Martinez-Forero I, Friedl P, Melero I. Anti-CD137 monoclonal antibodies and adoptive T cell therapy: a perfect marriage? Cancer Immunol Immunother 2016;65: 493–7.
29. Weigelin B, Bolanos E, Teijeira A, Martinez-Forero I, Labiano S, Azpilikueta A, et al. Focusing and sustaining the antitumor CTL effector killer response by agonist anti-CD137 mAb. PNAS 2015;112:7551–6.
30. Martinez-Forero I, Azpilikueta A, Bolanos-Mateo E, Nistal-Villan E, Palazon A, Teijeira A, et al. T cell costimulation with anti-CD137 monoclonal antibodies is mediated by K63-polyubiquitin-dependent signals from endosomes. J Immunol 2013;190:6694–706.
31. Rabu C, Quemener A, Jacques Y, Echasserieau K, Vusio P, Lang F. Production of recombinant human trimeric CD137L (4–1BBL). Cross-linking is essential to its T cell co-stimulation activity. J Biol Chem 2005;280:41472–81.
32. Sukumar M, Liu J, Mehta GU, Patel SJ, Roychoudhuri R, Crompton JG, et al. Mitochondrial membrane potential identifies cells with enhanced stemness for cellular therapy. Cell metabolism 2016;23:63–76.
33. Mishra P, Chan DC. Metabolic regulation of mitochondrial dynamics. J Cell Biol 2016;212:379–87.
34. Wai T, Langer T. Mitochondrial dynamics and metabolic regulation. Trends Endocrinol Metab 2016;27:105–17.
35. Lee HW, Nam KO, Park SJ, Kwon BS. 4–1BB enhances CD8+ T cell expansion by regulating cell cycle progression through changes in expression of cyclins D and E and cyclin-dependent kinase inhibitor p27kip1. Eur J Immunol 2003;33:2133–41.
36. Melero I, Shuford WW, Newby SA, Aruffo A, Ledbetter JA, Hellstrom KE, et al. Monoclonal antibodies against the 4–1BB T-cell activation molecule eradicate established tumors. Nat Med 1997;3:682–5.
37. Eun SY, Lee SW, Xu Y, Croft M. 4–1BB ligand signaling to T cells limits T cell activation. J Immunol 2015;194:134–41.
38. Starck L, Scholz C, Dorken B, Daniel PT. Costimulation by CD137/4–1BB inhibits T cell apoptosis and induces Bcl-xL and c-FLIP(short) via phosphatidylinositol 3-kinase and AKT/protein kinase B. Eur J Immunol 2005;35:1257–66.
39. So T, Croft M. Regulation of PI-3-Kinase and Akt Signaling in T lymphocytes and other cells by TNFR family molecules. Front Immunol 2013;4:139.
40. Sabbagh L, Andreeva D, Laramee GD, Oussa NA, Lew D, Bisson N, et al. Leukocyte-specific protein 1 links TNF receptor-associated factor 1 to survival signaling downstream of 4–1BB in T cells. J Leukoc Biol 2013;93:713–21.
41. Klein Geltink RI, O'Sullivan D, Corrado M, Bremser A, Buck MD, Buescher JM, et al. Mitochondrial priming by CD28. Cell 2017;171: 385–97 e11.
42. Melero I, Bach N, Hellstrom KE, Aruffo A, Mittler RS, Chen L. Amplification of tumor immunity by gene transfer of the co-stimulatory 4–1BB ligand: synergy with the CD28 co-stimulatory pathway. Eur J Immunol 1998;28:1116–21.
43. Hui E, Cheung J, Zhu J, Su X, Taylor MJ, Wallweber HA, et al. T cell costimulatory receptor CD28 is a primary target for PD-1-mediated inhibition. Science 2017;355:1428–33.

44. Sanmamed MF, Pastor F, Rodriguez A, Perez-Gracia JL, Rodriguez-Ruiz ME, Jure-Kunkel M, et al. Agonists of co-stimulation in cancer immunotherapy directed against CD137, OX40, GITR, CD27, CD28, and ICOS. Semin Oncol 2015;42:640–55.
45. van der Windt GJ, Everts B, Chang CH, Curtis JD, Freitas TC, Amiel E, et al. Mitochondrial respiratory capacity is a critical regulator of CD8+ T cell memory development. Immunity 2012;36:68–78.
46. Delgoffe GM. Filling the tank: keeping antitumor T cells metabolically fit for the long haul. Cancer Immunol Res 2016;4:1001–6.
47. Scharping NE, Menk AV, Whetstone RD, Zeng X, Delgoffe GM. Efficacy of PD-1 blockade is potentiated by metformin-induced reduction of tumor hypoxia. Cancer Immunol Res 2017;5:9–16.
48. Parra V, Verdejo HE, Iglewski M, Del Campo A, Troncoso R, Jones D, et al. Insulin stimulates mitochondrial fusion and function in cardiomyocytes via the Akt-mTOR-NFkappaB-Opa-1 signaling pathway. Diabetes 2014;63:75–88.
49. Wang C, Singer M, Anderson AC. Molecular dissection of CD8(+) T-cell dysfunction. Trends Immunol 2017;38:567–76.
50. Harao M, Forget MA, Roszik J, Gao H, Babiera GV, Krishnamurthy S, et al. 4-1BB-Enhanced expansion of CD8(+) TIL from triple-negative breast cancer unveils mutation-specific CD8(+) T Cells. Cancer Immunol Res 2017;5:439–45.
51. Mills EL, Kelly B, O'Neill LAJ. Mitochondria are the powerhouses of immunity. Nat Immunol 2017;18:488–98.